

Dynamics of a low-threshold optically pumped organic vertical-cavity surface-emitting laser

Mohammad Reza Shayesteh¹ · Ghafar Darvish¹

Received: 12 September 2015 / Accepted: 5 January 2016 / Published online: 28 January 2016
© The Author(s) 2016. This article is published with open access at Springerlink.com

Abstract We propose a low-threshold optically pumped organic vertical-cavity surface-emitting laser (OVCSEL). This device has the capability to apply both electrical and optical excitation. The microcavity structure consists of an organic light emitting diode with field-effect electron transport inserted in a high-quality factor double distributed Bragg reflector. The simulated quality factor of the microcavity is shown to be as high as 16,000. Also, we investigate threshold behaviour and the dynamics of the optically pumped OVCSEL with sub-picosecond pulses. Results from numerical simulation show that lasing threshold is $12.8 \text{ pJ}/0.64 \mu\text{J cm}^{-2}$ when pumped by sub-picosecond pulses of $\lambda = 400 \text{ nm}$ wavelength light.

Keywords Organic semiconductor · Organic vertical-cavity surface-emitting laser (OVCSEL) · Optical pump · Quality factor · Lasing threshold

Introduction

Organic semiconductor lasers provide superior features such as flexibility, accessibility of all wavelengths in the visible spectrum, and possibility of low cost and large-area

fabrication. These properties would make organic semiconductor lasers suitable for many applications in bioanalytics, digital printing, and fluorescence spectroscopy [1]. Although the first optically pumped organic laser has been demonstrated as early as 1996 [2], an electrically pumped organic laser has not been realized yet. Low charge carrier mobility, bimolecular annihilations process, induced absorption process, field quenching, and metal contact losses are the important factors that prevent lasing. Moreover, electrode contact absorption losses are most common losses in organic laser diodes. To develop an effective electrically pumped organic laser, one part of the strategy is lowering the optical losses. The various optically pumped organic microcavity geometries such as double distributed Bragg reflectors (DBRs) [3, 4], distributed feedback structures [5, 6], 2D photonic crystals [7, 8], photonic band gap fiber resonators [9], photonic crystal nanobeam cavity [10], and high contrast grating (HCG)-based microcavity [11] have been demonstrated. For optically pumped organic laser, microcavity with a high-quality factor leads to a lower optical power input. Chakaroun et al. proposed a high-quality factor microcavity organic laser for electrical pumping [12]. They have used high-reflection and low-absorption DBR mirror layers for reaching high-quality factor.

In this paper, we propose a low-threshold OVCSEL which has the feasibility to apply both electrical and optical pumping. The extended microcavity structure consists of an organic light emitting diode (OLED) with field-effect electron transport [13] set in between DBR mirrors. We also model the threshold behaviour and the dynamics of the OVCSEL optically pumped with sub-picosecond pulses. The results of optical pump-out will help us to estimate the injection current density value for electrical pumping.

✉ Ghafar Darvish
darvish_gh@srbiau.ac.ir

Mohammad Reza Shayesteh
m_shayesteh45@yahoo.com

¹ Department of Electrical Engineering, Science and Research Branch, Islamic Azad University, Tehran, Iran

Organic VCSEL structure design

The schematic structure of the proposed OVCSEL is shown in Fig. 1. The OLED with field-effect electron transport has been used as the active region. In our device structure, the metallic top contact is remote from the light-emission zone. As a result, the additional losses due to absorption photon at the metal contact can be decreased. Therefore, the quality factor of the microcavity that is inversely proportional to the cavity loss coefficient can be increased. The exciton density at the laser threshold (N_{th}) is reduced with a high-quality factor. The active region consists of several organic layers, including the host–guest system of tris-(8-hydroxyquinoline) aluminum (Alq_3) doped with 4-(dicyanomethylene)-2-methyl-6-(*p*-dimethylaminos-tyryl)-4H-pyran (DCM) with a thickness of 40 nm as the emission layer (EML), *N,N'*-ditridecylperylene-3,4,9,10-tetracarboxylic diimide (PTCDI- $C_{13}H_{27}$) with a thickness of 40 nm as the electron transport (ETL) and hole blocking (HBL) layer, and poly(triarylamine) (PTAA) with a thickness of 80 nm as the hole transport layer (HTL). The host–guest system as the emission layer has several advantages: (1) the host molecules efficiently absorb the pump light and non-radiatively transfer it via a Förster process to the guest molecules with efficiency of more than 90 % [14] and (2) the low concentration of the guest molecules reduces bimolecular annihilation and hence lowers the laser threshold.

The chosen anode is an indium tin oxide (ITO) (12 nm)/Ag (6 nm)/ITO (12 nm) to decrease the sheet resistance and support both hole injection and transparency. Also, we used the Al (100 nm) as the cathode to support a better electron injection. Ta_2O_5/SiO_2 as DBR layers provide high reflection and low absorption. Therefore, 12 and 11 pairs of Ta_2O_5/SiO_2 layers with a quarter wavelength optical thickness for each layer are used as the bottom mirror and

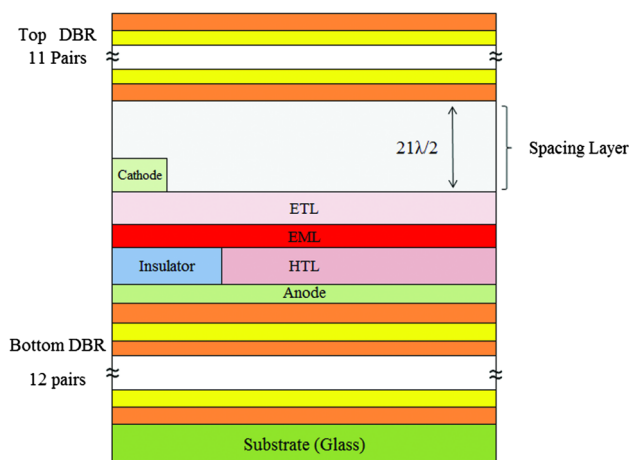


Fig. 1 Schematic structure of the proposed OVCSEL device

top mirror, respectively. To improve the quality factor, a matching layer (or spacer) with a thickness of a multiple of $\lambda/2$ between the active region and the top mirror has been used. The spacing layer can be a dielectric layer or more simply air or nitrogen if the top mirror is mounted on micromanipulators. As a result of optical modeling of the transmission spectrum, the thickness of spacing layer is derived to be 6510 nm corresponding to $21\lambda/2$ at $\lambda = 620$ nm.

For the fabrication of the device structure, the bottom mirror could be made by ion beam assisted deposition (IBAD) method on the glass substrate. Then, deposition of the OLED layers onto the bottom mirror is performed. Accurate alignment of the metallic cathode is obtained using an integrated shadow mask technique and angled deposition of the aluminum layer. To prevent the destruction of the organic layers due to the top mirror deposition, the fabricated top mirror is placed closer to the rest of the device using a micro-positioning to control its position [12].

For electrical excitation case, when an electric current is injected to the device, electrons are injected from cathode into ETL layer. The EML layer on top of the insulator is depleted of holes. The lowest unoccupied molecular orbital (LUMO) offset at the interface between EML and ETL prevents electron injection from ETL into EML. As a result, the depleted EML on top of the insulator behaves as a dielectric layer in series to the insulator, and an electron accumulation layer is formed in the ETL at the interface with EML. These electrons are transported laterally by the electric field from the cathode towards the recombination zone, i.e. the insulator edge. Hence, a micrometer-sized distance between the cathode and the light-emission zone is bridged by electrons with enhanced field-effect mobility. Near the insulator edge, electrons are injected into the EML, where they recombine with holes, injected from the anode and transported vertically through HTL. The exciton formation occurs and then radiative relaxation of these excitons to the ground state results in light-emission near the insulator edge, at a micrometer-sized distance from the metallic contact [13]. In this way, the proposed OVCSEL allows to minimize optical losses at the metal cathode.

Theoretical modeling

In this section, we investigate the dynamics of the OVCSEL optically pumped with sub-picosecond pulses. The high-quality factor and the sub-picosecond pulses pump avoid relaxation oscillation. Therefore, lasing in the OVCSEL can be modeled using the following rate equations [10, 15]:

$$\frac{dN_A(t)}{dt} = -\frac{N_A(t)}{\tau_A} - \frac{N_A(t)}{\tau_F} \tag{1}$$

$$\frac{dN_D(t)}{dt} = \frac{N_A(t)}{\tau_F} - \frac{N_D(t)}{\tau_D} - C\sigma_{se}N_D(t)N_P(t) \tag{2}$$

$$\frac{dN_P(t)}{dt} = \Gamma C\sigma_{se}N_D(t)N_P(t) - \frac{N_P(t)}{\tau_{cav}} + \Gamma\beta\frac{N_D(t)}{\tau_{D,r}} \tag{3}$$

where N_A and N_D denote the excited state density of Alq₃ and DCM, respectively, while N_P represents the photon density of the lasing mode. Equation (1) describes the dynamics of the Alq₃ molecules. The first term represents the loss mechanism due to radiative and nonradiative decay. The last term represents the loss mechanism due to Förster resonant energy transfer (FRET) to DCM molecules. Due to the delta-like pumping, the initial excited state density of Alq₃ is $\eta E_{in}/h\nu_p v_{exc}$, where E_{in} is the pump energy density, η is fraction of energy absorbed by the film, ν_p is the pump frequency, h is Planck constant, and v_{exc} is excitation volume. We also assume that excitation spot size is 50 μm and the area of incident beam is $20 \times 10^{-6} \text{ cm}^2$.

Equation (2) describes the dynamics of DCM molecules. The first term denotes the rate at which the DCM excitons are created due to FRET process. The second term accounts for the losses of excitons due to radiative and nonradiative decay. The third term accounts for the simulated photons; σ_{se} is the stimulated emission cross section of DCM, and c is the vacuum speed of light.

Equation (3) describes the dynamics for photon in the lasing mode. The first term is proportional to number of stimulated emitted photons with the power confinement factor Γ . Power confinement factor was calculated using FDTD simulation to be 0.3 for the fundamental mode. The second term includes all cavity losses with the cavity lifetime (τ_{cav}), which is calculated from $\tau_{cav} = Q/2\pi\nu$. The last term represents the spontaneous emission photons into the laser mode with β as fraction emitted into the laser mode.

Simulation results

The reflectance spectrum of the mirrors is shown in Fig. 2. The mirrors were designed to have a maximum reflectivity at the central emission wavelength of the active region, i.e. $\lambda_0 = 620 \text{ nm}$ which is the peak emission of the Alq₃:DCM guest–host system [16]. The simulated transmission spectrum of the microcavity which is calculated using transfer matrix method (TMM) is shown in Fig. 3. This figure shows that the microcavity exhibits only one transmission peak within the photoluminescence spectrum of Alq₃:DCM and a quality factor up to 16,000. Indeed, the satellite transmissions peaks are located outside of the

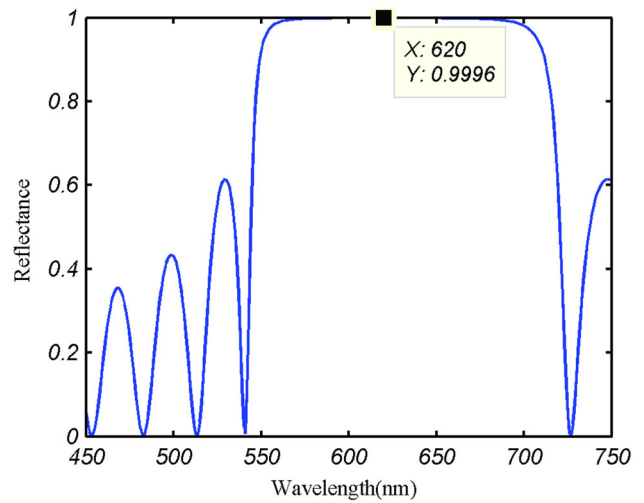


Fig. 2 Reflectance spectrum of the DBR mirror consists of 12 pairs of Ta₂O₅/SiO₂ layers

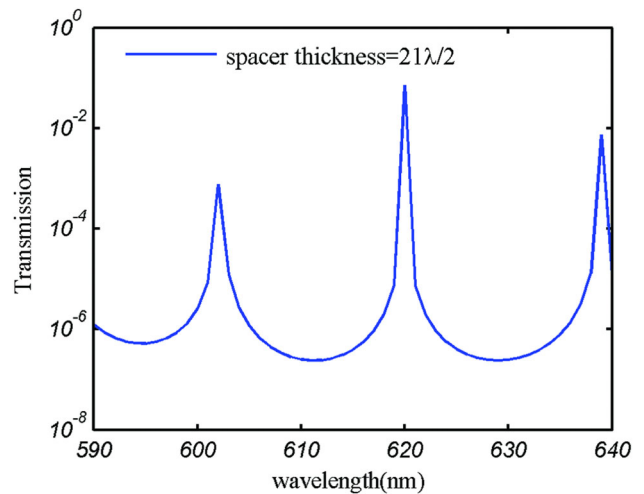


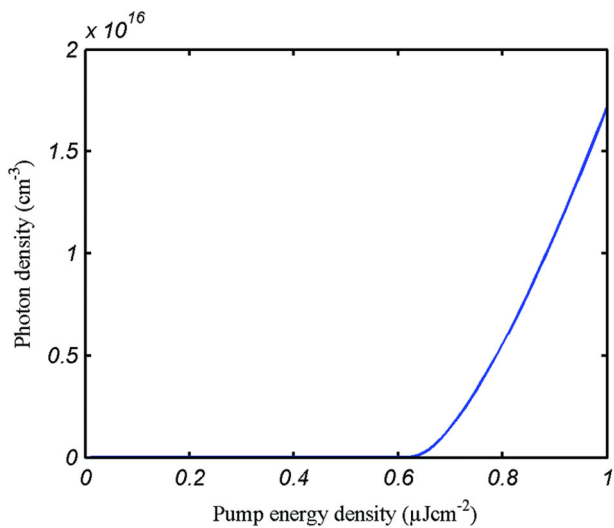
Fig. 3 Calculated transmission spectrum of the microcavity using TMM

photoluminescence spectrum of Alq₃:DCM. Therefore, the dynamic single-mode operations can be obtained.

For laser emission, the device is optically pumped by pulse lengths of about 200 fs, and the optical pump wavelength of $\lambda = 400 \text{ nm}$ is considered. When wavelength of optical pump is 400 nm, the microcavity will have low reflection for a large range of incident angles. To evaluate the results, the coupled Eqs. (1)–(3) are numerically solved with initial condition by a fourth-order Runge–Kutta algorithm. The simulation parameters are given in Table 1. The quality factor and confinement factor of the microcavity are determined using numerical simulation. In the calculation the materials are characterized by complex refractive indices. Other parameters such as radiative

Table 1 Device parameters used in the numerical simulation [10, 11, 13]

Symbol	Parameter	Value
λ	Lasing wavelength	620 nm
τ_D	Radiative and non-radiative relaxations time for guest molecules	1.3 ns
$\tau_{D,r}$	Radiative lifetime	5 ns
τ_F	Förster transfer time	10 ps
τ_A	Radiative and non-radiative relaxations time for host molecules	16 ns
β	Spontaneous emission coupling factor	1×10^{-4}
Q	Quality factor of microcavity	16,000
σ_{SE}	Stimulated emission cross section	$1 \times 10^{-16} \text{ cm}^2$
Γ	Confinement factor	0.3
η	Fraction of absorbed light	0.9

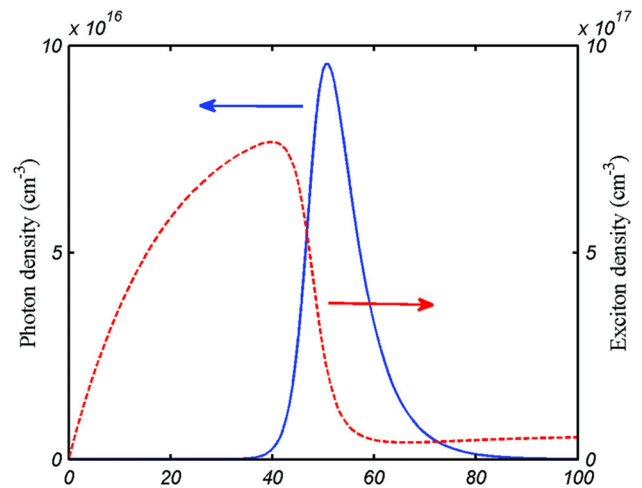
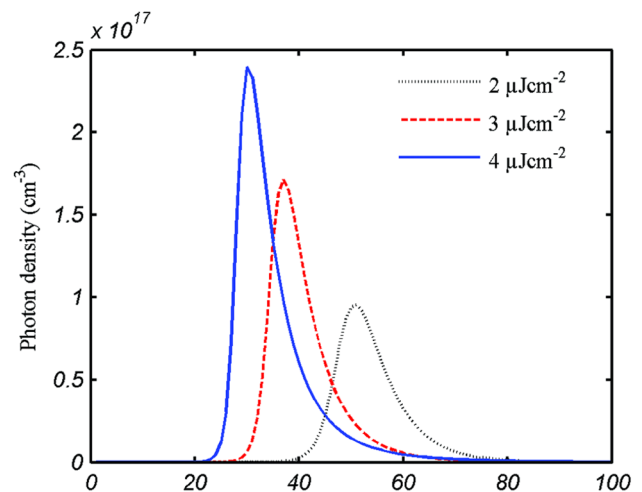
**Fig. 4** Photon density peak versus pump energy densities

lifetime, Förster transfer time, and spontaneous emission coupling factor, etc., are values from the literature.

Figure 4 shows the photon density peak versus pump energy densities. This plot shows threshold at pulse energy density of about $0.64 \mu\text{J cm}^{-2}$ (pump energy = 12.8 pJ). Figure 5 shows the photon density and the exciton density versus time for pump energy density of $2 \mu\text{J cm}^{-2}$, which is above threshold. As can be seen in this figure, the excitons increase fast; however, the photon density rises to its peak when exciton density decreases abruptly.

Figure 6 shows the photon density versus time for different pump energy densities above the threshold. As one can see, both delay and output pulse width decrease with higher pump energy density, as it is well known for optical gain-switched inorganic semiconductor VCSEL and has been demonstrated already [17, 18].

For electrical excitation, the current density needed to achieve the same pumping which is required for lasing in the optical pumped structure can be calculated by [19]

**Fig. 5** Temporal evolution of the photon and exciton density for pump energy density of $2 \mu\text{J cm}^{-2}$ **Fig. 6** Photon density versus time for different pump energy densities

$$J_{\text{th}} = \frac{2ne}{\chi\tau_D} \quad (4)$$

where n is number of excitons formed in the emission layer and e is the electron charge. χ is the ratio of radiative singlet excitons to the total number of excitons formed by electrical injection, which is assumed to be 0.25. Using Eq. (4), the electrical current density is 55 A cm^{-2} for lasing threshold.

In this work, we have focused on design and simulation of a high-quality optical microcavity toward the development of an electrical pumped organic laser. In this context, it has to be noted that the optical properties of these structures depend on the preparation technique. However, practical works are under progress to demonstrate the feasibility of such devices.

Conclusion

In this paper, we have proposed a low-threshold optically pumped organic vertical-cavity surface-emitting laser. The device has the feasibility to apply both electrical and optical pumping. Moreover, the device exhibits several characteristics that promise to respect to the realization of an electrically pumped organic laser. The reduction optical losses due to the remoteness of the metallic cathode are the most important ones. The laser microcavity structure consists of an OLED with field-effect electron transport inserted in a high-quality factor double DBR. The simulated quality factor of the microcavity which has been calculated using transfer matrix method (TMM) is as high as 16,000. Also, we have investigated the threshold behaviour and ultrafast dynamics of the OVCSEL optically pumped with sub-picosecond pulses. Results from numerical simulation show that lasing threshold is of about $12.8 \text{ pJ}/0.64 \text{ } \mu\text{J cm}^{-2}$ when pumped by sub-picosecond pulses of $\lambda = 400 \text{ nm}$ wavelength light. This optically pumped laser threshold would correspond to a laser current density as high as 55 A cm^{-2} . Therefore, this structure might be a promising route towards the realization of an electrically pumped organic laser.

Open Access This article is distributed under the terms of the Creative Commons Attribution 4.0 International License (<http://creativecommons.org/licenses/by/4.0/>), which permits unrestricted use, distribution, and reproduction in any medium, provided you give appropriate credit to the original author(s) and the source, provide a link to the Creative Commons license, and indicate if changes were made.

References

- Gartner, C., Karnutsch, C., Pflumm, C., Lemmer, U.: Numerical device simulation of double-heterostructure organic laser diodes including current-induced absorption processes. *IEEE J. Quantum Electron.* **43**, 1006–1017 (2007)
- Tessler, N., Denton, G.J., Friend, R.H.: Lasing from conjugated-polymer microcavities. *Nature* **382**, 695–697 (1996)
- Kena-Cohen, S., Forrest, S.: Room-temperature polariton lasing in an organic single-crystal microcavity. *Nat. Photonics* **4**, 371–375 (2010)
- Akselrod, G.M., Young, E.R., Bradley, M.S., Bulovic, V.: Lasing through a strongly-coupled mode by intra-cavity pumping. *Opt. Express* **21**, 12122–12128 (2013)
- Schneider, D., Rabe, T., Riedl, T., Dobbertin, T., Kroger, M., Becker, E., Johannes, H., Kowalsky, W., Weimann, T., et al.: Laser threshold reduction in an all-spiro guest-host system. *Appl. Phys. Lett.* **85**, 1659–1661 (2004)
- Rose, A., Zhu, Z., Madigan, C.F., Swager, T.M., Bulovic, V.: Sensitivity gains in chemo sensing by lasing action in organic polymers. *Nature* **434**, 876–879 (2005)
- Riechel, S., Wittwer, V., Scherf, U.: A nearly diffraction limited surface emitting conjugated polymer laser utilizing a two-dimensional photonic band structure. *Appl. Phys. Lett.* **77**, 2310–2312 (2000)
- Gourdon, F., Chakaroun, M., Fabre, N., Solard, J., Cambril, E., Yacomotti, A.M., Bouchoule, S., Fischer, A., Boudrioua, A.: An optically pumped lasing from organic two-dimensional planar photonic crystal microcavity. *Appl. Phys. Lett.* **100**, 213304–213307 (2012)
- Shapira, O., Kuriki, K., Orf, N.D., Abouraddy, A.F., Benoit, G., Viens, J.F., Rodriguez, A., Ibanescu, M., Joannopoulos, J.D., Fink, Y., et al.: Surface-emitting fiber lasers. *Opt. Express* **14**, 3929–3935 (2006)
- Deotare, P.B., Mahony, T.S., Bulovic, V.: Ultracompact low-threshold organic laser. *ACS Nano* **8**, 11080–11085 (2014)
- Shayesteh, M.R., Darvish, G., Ahmadi, V.: A low-threshold high-index-contrast grating (HCG)—based organic VCSEL. *Opt. Laser Technol.* **75**, 173–176 (2015)
- Chakaroun, M., Cons, A., Fabre, N., Gourdon, F., Solard, J., Fischer, A., Boudrioua, A., Lee, C.C.: Optimal design of a microcavity organic laser device under electrical pumping. *Opt. Express* **19**, 493–505 (2011)
- Schols, S., Verlaak, S., Rolin, C., Cheyns, D., Genoe, J., Heremans, P.: An organic light-emitting diode with field-effect electron transport. *Adv. Funct. Mater.* **18**, 136–144 (2008)
- Zhong, G.Y., He, J., Zhang, S.T., Xu, Z., Xiong, Z.H., Shi, H.Z., Ding, X.M.: In situ photoluminescence investigation of doped Alq. *Appl. Phys. Lett.* **80**, 4846–4848 (2002)
- Koschorreck, M., Gehlhaar, R., Lyssenko, V.G., Swoboda, M., Hoffmann, M., Leo, K.: Dynamics of a high-Q vertical cavity organic laser. *Appl. Phys. Lett.* **87**, 181108–181110 (2005)
- Punke, M., Mozer, S., Stroisch, M., Gerken, M., Bastian, G., Lemmer, U.: Organic semiconductor devices for micro-optical application. *Proc. SPIE* **6185**(618505), 1–13 (2006)
- Melcer, L.G., Karin, J.R., Nagarajan, R., Bowers, J.E.: Picosecond dynamics of optical gain switching in vertical cavity emitting lasers. *IEEE J. Quantum Electron.* **27**(6), 1417–1425 (1991)
- Demokan, M.S., Nacaroglu, A.: An analysis of gain-switched semiconductor lasers generating pulse-code-modulated light with a high bit rate. *IEEE J. Quantum Electron.* **20**(9), 1016–1022 (1984)
- Kozlov, V.G., Parthasarathy, G., Burrows, P.E., Khalfin, V.B., Wang, J., Chou, S.Y., Forrest, S.R.: Structures for organic diode laser and optical properties of organic semiconductors under intense optical and electrical excitation. *IEEE J. Quantum Electron.* **36**, 18–26 (2000)

